AD-A115 834 PACIFIC-SIERRA RESEARCH CORP SANTA MONICA CA F/G 17/2.1
TRANSVERSE ELECTRIC WAVES FOR VLF/LF COMMUNICATION BETWEEN AIRC--ETC(U)
NOV 81 E C FIELD N00014-80-C-0398
UNCLASSIFIED PSR-1125 NL

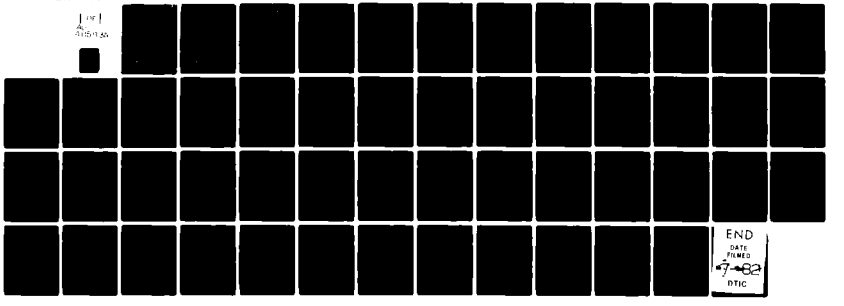

END
DATE FILMED
7-82
DTIC

(12)

PSR Report 1125

TRANSVERSE ELECTRIC WAVES FOR VLF/LF COMMUNICATION BETWEEN AIRCRAFT

E. C. Field, Jr.

November 1981

Final Technical Report
Contract N00014-80-C-0398

Sponsored by
Office of Naval Research
Earth and Environmental Physics Program
Arctic and Earth Sciences Division
800 North Quincy Street
Arlington, Virginia 22217

PACIFIC • SIERRA RESEARCH CORP.
12340 Santa Monica Blvd. ○ Los Angeles, California 90025

PSR Report 1125

TRANSVERSE ELECTRIC WAVES FOR VLF/LF COMMUNICATION BETWEEN AIRCRAFT

E. C. Field, Jr.

November 1981

Final Technical Report
Contract N00014-80-C-0398

Sponsored by
Office of Naval Research
Earth and Environmental Physics Program
Arctic and Earth Sciences Division
800 North Quincy Street
Arlington, Virginia 22217

PACIFIC • SIERRA RESEARCH CORP.
12340 Santa Monica Blvd. ° Los Angeles, California 90025

SECURITY CLASSIFICATION OF THIS PAGE (When Data Entered)

REPORT DOCUMENTATION PAGE

READ INSTRUCTIONS BEFORE COMPLETING FORM

1. REPORT NUMBER: PSR Report 1125	2. GOVT ACCESSION NO.: AD-A115 834
3. RECIPIENT'S CATALOG NUMBER:	
4. TITLE (and Subtitle): TRANSVERSE ELECTRIC WAVES FOR VLF/LF COMMUNICATION BETWEEN AIRCRAFT	5. TYPE OF REPORT & PERIOD COVERED: Final Technical Report, April 1980 - October 1981
	6. PERFORMING ORG. REPORT NUMBER: PSR Report 1125
7. AUTHOR(s): E. C. Field, Jr.	8. CONTRACT OR GRANT NUMBER(s): N00014-80-C-0398
9. PERFORMING ORGANIZATION NAME AND ADDRESS: Pacific-Sierra Research Corporation, 1456 Cloverfield Boulevard, Santa Monica, California 90404	10. PROGRAM ELEMENT, PROJECT, TASK AREA & WORK UNIT NUMBERS: NR 089-156
11. CONTROLLING OFFICE NAME AND ADDRESS	12. REPORT DATE: November 1981
	13. NUMBER OF PAGES: 40
14. MONITORING AGENCY NAME & ADDRESS(if different from Controlling Office): Office of Naval Research, Code 414J, Arlington, Virginia 22217	15. SECURITY CLASS. (of this report): Unclassified
	15a. DECLASSIFICATION/DOWNGRADING SCHEDULE

16. DISTRIBUTION STATEMENT (of this Report)

Approved for public release and sale: distribution unlimited.

17. DISTRIBUTION STATEMENT (of the abstract entered in Block 20, if different from Report)

18. SUPPLEMENTARY NOTES

19. KEY WORDS (Continue on reverse side if necessary and identify by block number)

VLF/LF propagation
VLF/LF communication

20. ABSTRACT (Continue on reverse side if necessary and identify by block number)

This report compares the excitation and propagation of VLF/LF transverse electric (TE) and transverse magnetic (TM) long waves in the earth-ionosphere waveguide. It calculates the dependence of TE and TM mode parameters on three factors: (1) ground conductivity, (2) state of the ionosphere, and (3) elevation of terminals above the ground. It also briefly addresses the effects of atmospheric noise and ground-based jammers on the performance of TE links. Results are given for frequencies between 20 and 50 kHz.

DD FORM 1473 EDITION OF 1 NOV 65 IS OBSOLETE

SECURITY CLASSIFICATION OF THIS PAGE (When Data Entered)

.OOC 1

BLOCK 20--Cont.

Only TM signals are efficiently radiated by ground-based transmitters. However, TE signals are strongly excited by nearly horizontal trailing-wire antennas at elevations exceeding 20 kft and, thus, can be important for air-to-air links. Poorly conducting ground heavily degrades TM propagation, but it will not affect TE propagation if the terminals are elevated at least 5000 ft. TE signals are, therefore, better suited than TM signals for air-to-air links that traverse Greenland and much of Canada. For paths over highly conducting ground, TM signals suffer less degradation than TE signals during intense disturbances; for ground conductivities less than about ~~10^{-4}~~ mhos/m, however, TM signals are more adversely affected. TE signals also provide protection against ground-based jammers under disturbed ionospheric conditions where geomagnetic conversion is slight.

PREFACE

This report analyzes the propagation of horizontally (TE) and vertically (TM) polarized VLF/LF signals between airborne terminals. Signal dependence on ground conductivity, state of the ionosphere, and aircraft elevation is calculated. The results are applicable to links between airborne transmitters and TACAMO VLF/LF relay aircraft.

Portions of this report were presented at the Meeting of the Electromagnetic Wave Propagation Panel (Medium, Long and Very Long Wave Propagation) of the North Atlantic Treaty Organization (NATO) Advisory Group for Aerospace Research and Development (AGARD) held in Brussels, Belgium, 21-25 September 1981.

SUMMARY

This report compares the excitation and propagation of VLF/LF transverse electric (TE) and transverse magnetic (TM) long waves in the earth-ionosphere waveguide. It calculates the dependence of TE and TM mode parameters on three factors: (1) ground conductivity, (2) state of the ionosphere, and (3) elevation of terminals above the ground. It also briefly addresses the effects of atmospheric noise and ground-based jammers on the performance of TE links. Results are given for frequencies between 20 and 50 kHz.

Only TM signals are efficiently radiated by ground-based transmitters. However, TE signals are strongly excited by nearly horizontal trailing-wire antennas at elevations exceeding 20 kft and, thus, can be important for air-to-air links. Poorly conducting ground heavily degrades TM propagation, but it will not affect TE propagation if the terminals are elevated at least 5000 ft. TE signals are, therefore, better suited than TM signals for air-to-air links that traverse Greenland and much of Canada. For paths over highly conducting ground, TM signals suffer less degradation than TE signals during intense disturbances; for ground conductivities less than about 10^{-4} mhos/m, however, TM signals are more adversely affected. TE signals also provide protection against ground-based jammers under disturbed ionospheric conditions where geomagnetic conversion is slight.

CONTENTS

FIGURES

I. INTRODUCTION

Trailing-wire transmitting antennas are used on airborne command posts and TACAMO very-low-frequency (VLF)/low-frequency (LF) relay aircraft. During high-speed operations, such antennas trail behind the aircraft in a nearly horizontal orientation, causing most of the radiated energy to be horizontally polarized. Because the resulting transverse electric (TE) energy could play an important role in communication links between command post and TACAMO aircraft, Pacific-Sierra Research Corporation (PSR) has investigated the potential benefits to be gained from exploiting such energy.

The present report compares the propagation of TE and transverse magnetic (TM) long waves in the earth-ionosphere waveguide. It calculates the dependence of TE and TM mode parameters on three factors: (1) ground conductivity, (2) state of the ionosphere, and (3) elevation of terminals above the ground. Results are given for frequencies between 20 and 50 kHz, which include the most commonly used portions of the VLF and LF bands.

Before air-to-air links were deployed, VLF/LF communications were carried out with at least one--and often both--terminals on the ground or in the sea. Under such conditions, only TM signals are excited efficiently enough to be of interest. Because they have been used longer, TM signals have been more thoroughly analyzed and measured than TE signals. However, a fair amount of experimental and analytic work has been done on TE mode properties. Lewis and Harrison [1975] used a balloon-borne probe to measure a strong TE polarized wave from an airborne LF transmitter. More recent rocket-borne measurements of signals from airborne transmitters have yielded TE height-gain profiles across the entire width of the earth-ionosphere waveguide [Kossey et al., 1981]. Pappert [1970] computed the mode excitation by horizontal dipoles under normal ionospheric conditions. Field [1975] and Field et al. [1976] calculated the TE mode structure and signal strength from airborne transmitters under normal and disturbed ionospheric conditions.

Kossey et al. [1981] have summarized the available experimental and theoretical information on TE signals.

The research cited above suggests that TE signals offer the following benefits for air-to-air links:

- Efficient excitation by nearly horizontal trailing wires.
- Filling of TM interference nulls.
- Protection against ground-based jammers.
- Low atmospheric noise.
- No degradation by poorly conducting ground, such as exists throughout Greenland and much of Canada.

The greatest potential disadvantages of TE mode links are that they (1) are more vulnerable than TM modes to degradation in disturbed environments; (2) do not propagate quite as well as TM modes under normal conditions; and (3) exhibit a transmission pattern that has a null in the end-fire direction. (The first two items do not apply in the case of propagation over low-conductivity ground.)

Despite the progress in research on TE signals, the benefits to be derived from adding a TE capability to aircraft have not been fully assessed. Experiments on TE propagation need to be extended to paths traversing regions where the ionosphere is disturbed or ground conductivity is low. More measurements of TE atmospheric noise are also required to properly evaluate system performance. Theoretical analyses should be extended to (1) treat propagation over poorly conducting ground when the ionosphere is disturbed, (2) account for differences between TE and TM noise when comparing systems, and (3) determine how well a ground-based jammer can exploit geomagnetic conversion as a means of creating horizontally polarized interference at aircraft altitudes, particularly when only part of the path is disturbed.

This report, which concentrates on TE/TM performance under disturbed conditions, gives detailed theoretical results for the dependence on ground conductivity. It also briefly considers the effects of TE atmospheric noise. Geomagnetic conversion of vertically

polarized jamming signals can be important when much of the propagation path is undisturbed, but not when the widespread disturbances considered in this report are operative. Therefore, it is excluded from the analysis.

II. PROPAGATION EQUATIONS

The detailed equations governing VLF propagation have appeared elsewhere (e.g., Galejs [1972], Wait [1970], Field et al. [1976]), so need not be repeated here. We solve them numerically, using the method of Field et al. [1976], accounting for the vertical inhomogeneity of the ionosphere and curvature of the earth. To define the notation and illustrate the key dependences, we recapitulate the equations that govern the electric field when geomagnetic anisotropy can be neglected. That approximation is very accurate when the upper boundary of the earth-ionosphere waveguide is depressed far below its normal level; and it is fairly accurate for long-range propagation under normal daytime conditions.

The TM and TE waveguide modes do not exist independently when geomagnetic anisotropy is important. Instead, they are coupled, with the TM mode having a horizontally polarized component and the TE mode a vertically polarized component. Under such conditions, vertical and horizontal electric dipole antennas will excite *both* TM and TE waveguide modes. That geomagnetic coupling is most pronounced when significant amounts of energy penetrate to--and are reflected from--altitudes above about 75 km, where the gyrofrequency exceeds the collision frequency. Such high reflection altitudes can occur (1) on short paths where the waves are steeply incident on the ionosphere, or (2) during normal nighttime, when the ionospheric D-layer is rarefied. This report concentrates on disturbed conditions, and therefore does not address conditions of substantial geomagnetic coupling.

TRANSVERSE MAGNETIC MODES

Typically, VLF/LF transmitters are vertically oriented, and their fields are composed of a superposition of TM modes. The vertical electric field is given by

$$E_V = -120\pi i\, e^{-\pi i/4}\, \frac{IL \cos\psi}{\sqrt{\lambda d}} \sqrt{\frac{d/a}{\sin d/a}} \sum_{\ell} S_\ell^{3/2}\, \Lambda_\ell \exp\left(-\frac{\beta_\ell d}{8.7}\right)$$

$$\times \exp\left(-\frac{2\pi i}{\lambda}\frac{c}{v_\ell} d\right) G_\ell(h_T) G_\ell(h_R) \quad \text{V/m} , \tag{1}$$

where the subscript ℓ denotes quantities associated with the ℓth TM mode, IL is the effective electric dipole moment of the transmitting antenna; λ is the free-space wavelength; d is the distance from the transmitter; a is the earth's radius; and c is the speed of light. We have included a factor cos ψ--where ψ is the angle between the dipole orientation and the vertical--to account for inclined transmitting antennas. Of course, cos ψ = 1 for a vertical electric dipole. Although most quantities are in MKS units, we express all distances (L, λ, d, a) in megameters.

The quantity S_ℓ is the eigenvalue of the ℓth TM mode. At VLF, however, S has a magnitude close to unity, so the term $S_\ell^{3/2}$ in Eq. (1) does not appreciably influence the field. The magnitude of the vertical electric field depends on the state of the ionosphere through three parameters: Λ_ℓ, the excitation factor for the TM mode; β_ℓ, the attenuation rate in decibels per megameter of propagation (dB/Mm); and G_ℓ, the height-gain function for transmitter and receiver heights h_T and h_R, respectively. The phase of the ℓth mode is governed by the relative phase velocity v_ℓ/c. These propagation parameters must all be computed numerically for model ionospheres having arbitrary height profiles.

TRANSVERSE ELECTRIC MODES

Airborne VLF/LF transmitters use trailing-wire antennas whose primary orientation is often horizontal. Such antennas radiate a complicated superposition of TM and TE modes. Here we avoid much of that complexity by considering broadside propagation, where the great-circle path connecting transmitter and receiver is perpendicular to the plane containing the inclined electric-dipole transmitting antenna.

The vertical electric field produced by the vertical component of the inclined transmitting antenna is given by Eq. (1). The broadside horizontal electric field produced by the horizontal component is given by

$$E_H = -120\pi i\, e^{-\pi i/4}\, \frac{IL \sin \psi}{\sqrt{\lambda d}} \sqrt{\frac{d/a}{\sin d/a}} \sum_m S_m^{-1/2}\, \Lambda_m \exp\left(-\frac{\beta_m d}{8.7}\right)$$

$$\times \exp\left(-\frac{2\pi i}{\lambda}\frac{c}{v_m} d\right) G_m(h_T) G_m(h_R) \quad \text{V/m} . \qquad (2)$$

The symbols are the same as in Eq. (1), except that m denotes the m*th* TE mode.

III. NORMAL AND DISTURBED IONOSPHERIC MODELS

Many types of ionospheric disturbances can affect VLF/LF propagation. X-rays from solar flares ionize the D- and E-layers of the ionosphere over the sunlit hemisphere. Energetic electrons and protons from solar particle events (SPE) ionize the polar cap at altitudes well below those from which ELF waves are usually reflected. High-altitude nuclear bursts produce various prompt and delayed ionizing radiations, including γ-rays, β-particles, and neutrons. The γ-rays penetrate to even lower altitudes than energetic protons from a strong SPE, and thus can cause much more severe distortions of the earth-ionosphere waveguide.

In this report, we concentrate on SPE and nuclear disturbances, which cause ionization well below the normal ionosphere. They constrict the earth-ionosphere waveguide, and usually degrade propagation. We do not consider disturbances--such as X-ray flares--that occasionally enhance propagation.

Figure 1 shows height profiles of electron and positive-ion density calculated from models of nominal nuclear environments consisting of widespread, high-altitude fission debris. The profiles shown are convenient for calculating the dependence of the waveguide propagation parameters on the intensity of a disturbance. They span a wide range of intensities, but, because propagation depends on ionization height gradient as well as intensity, they do not cover all possible cases. Specific events must therefore be analyzed individually. The "moderate" and "intense" profiles represent levels of ionization typical of strong SPEs as well as spread-debris environments. We can therefore use them to infer effects of both natural and man-made disturbances.

Before presenting the numerical results, we briefly review the relative importance of electrons and heavy ions. The geomagnetic field will be ignored for the disturbances considered here, since the most important processes occur at altitudes where the electron and ion

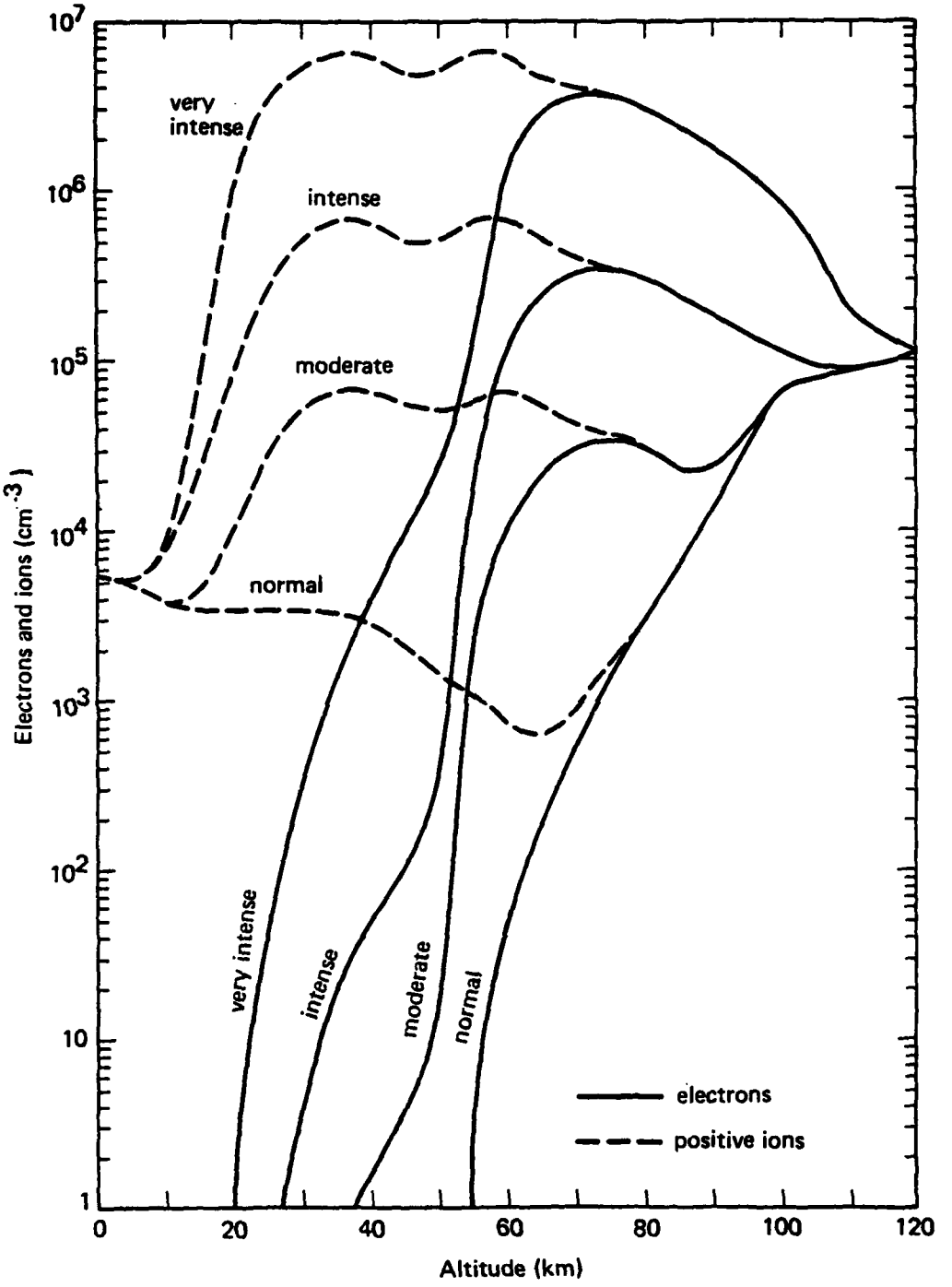

Fig. 1--Electron and ion density profiles for nominal daytime normal and disturbed environments

collision frequencies, ν_e and ν_i, exceed the corresponding gyrofrequencies. The ionospheric refractive-index height profile is thus the basic input to predictive codes. Electrons and many species of heavy ions contribute to the refractive index. In practice--as illustrated in Fig. 1--ionic species are classified simply as "positive" or "negative," each type having properties determined by averaging over the species actually present. Further, it is usually assumed that such generic ions have equal masses M_i and collision frequencies ν_i. The refractive index n then takes the simplified form

$$n^2 - 1 \approx -i \frac{q^2}{\omega \varepsilon_0 M_e \nu_e} \left(N_e + \frac{2 M_e \nu_e}{M_i \nu_i} N^+ \right) , \qquad (3)$$

where q is the electron charge, ω is the angular frequency, N_e is the electron density, and N^+ is the density of the "average" positive ion. The factor of two in Eq. (3) occurs because the positive- and negative-ion densities are nearly equal at altitudes where ions are important.

The values of M_i and ν_i at a given altitude are not well known. We use an atomic weight of 32 for M_i. However, depending on altitude, values as low as 19 or as high as 50 to 60 are possible. Similarly, ν_i could range anywhere from one-tenth to one-fortieth of ν_e. We follow current convention in assuming $\nu_i = \nu_e/20$, and use a nominal profile for ν_e (e.g., Pappert and Moler [1974]).

Figure 1 shows that ions greatly outnumber electrons at the lower altitudes, where they dominate propagation despite their larger mass. By inserting the assumed numerical values into Eq. (3), and then comparing the first and second terms in the parentheses, we find that a transition from electron to ion dominance occurs at the altitude where

$$N_e \sim \frac{N^\pm}{1500} . \qquad (4)$$

For the models shown in Fig. 1, this criterion implies that signals confined mainly to altitudes below, say, 50 to 55 km are more strongly

affected by ions than electrons. Of course, that transition altitude will shift if different values are assumed for either the masses or collision frequencies.

IV. STRUCTURE OF MODES

Equations (1) and (2) show that each mode's contribution to the total field is proportional to the product of four quantities: the excitation factor Λ, the transmitter height-gain function $G(h_T)$, the receiver height-gain function $G(h_R)$, and the propagation factor $\exp(-\beta d/8.7)$. This section gives calculated values of the four quantities for the model ionosphere* presented in Fig. 1 and a wide range of ground conductivities. For convenience, several figures have been reproduced from Field [1975] and Field et al. [1976].

HEIGHT-GAIN FUNCTIONS

The height-gain functions of a waveguide mode account for the transmitter and receiver elevations. A mode's contribution to the total field is proportional to the product of the excitation factor, the transmitter height-gain function, and the receiver height-gain function. The two latter functions are identical and, therefore, equal when both terminals are at the same altitude. In that case, a mode's relative importance at a given altitude is proportional to the product of the excitation factor and the square of the height-gain function.

Normal Daytime Conditions

Figure 2 shows the altitude dependence of the hieght-gain functions G_ℓ and G_m for the first three TM modes (ℓ = 1, 2, 3) and first two TE modes (m = 1, 2) for normal daytime conditions, $\sigma_g = 10^{-3}$ mhos/m, and a frequency of 20 kHz. These functions exhibit the classic height dependence for antennas over highly conductive ground. That is, the TM mode functions approximate unity over most of the waveguide, except for some rather sharp nulls; but, above a few kilometers, the TE mode functions increase sharply to values over 100.

---

*Some of the results given below are calculated from an exponential fit to the normal-daytime-conductivity height profile. Differences between these results and those from the actual profile are minor.

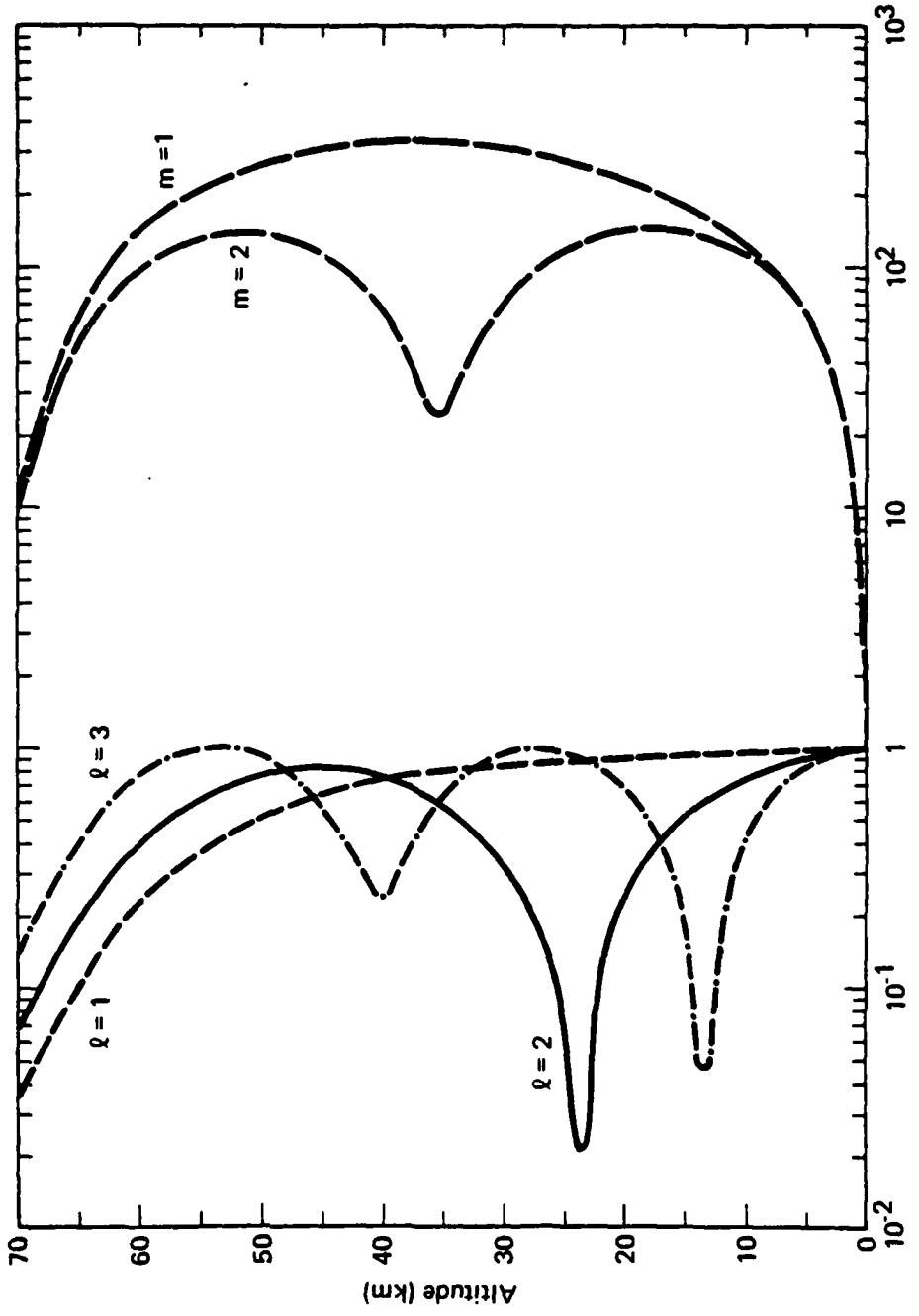

Fig. 2--Height-gain function versus altitude for first three TM modes and first two TE modes: normal daytime conditions, $\sigma = 10^{-3}$ mhos/m, and f = 20 kHz

At higher frequencies, the height profiles of $G_{\ell,m}$ resemble those shown in Fig. 2 for 20 kHz. The main difference is that the height-gain function of the first TM mode develops a broad maximum in the 40 to 60 km altitude range as the frequency increases above 30 kHz. Such "whispering gallery" behavior is not important for the ground-based and airborne terminals considered here, but could be significant for very high, balloon-borne terminals.

Effects of Ground Conductivity and Ionospheric Disturbances

Figure 3 shows the altitude dependence of the height-gain functions of the lowest TM and TE modes for a disturbance corresponding to either a fairly strong nuclear environment or very strong SPE. Higher order modes are severely attenuated by such a disturbance, and the lowest modes (ℓ,m = 1) are usually adequate to describe long-range signals. If we compare the curves labeled $\sigma = 10^{-3}$ mhos/m in Fig. 3 with the curves labeled ℓ,m = 1 in Fig. 2, we find that the main effect of the disturbance is to confine the height-gain functions to lower-than-normal altitudes.

Of greater importance is the dependence of the height-gain functions on ground conductivity. Figure 3 shows that--provided the terminals are not too near the ground--the TE height-gain function is nearly proportional to $\sigma^{1/2}$ and, therefore, varies greatly for the range of conductivities shown. In contrast to that behavior, the TM mode height-gain function depends only slightly on ground conductivity, particularly at altitudes below about 15 km which are accessible to airborne VLF terminals. Although calculated specifically for the intense disturbance, the dependence of height-gain functions on conductivity shown in Fig. 3 is typical of all ionospheric conditions considered in this report.

EXCITATION OF MODES

The excitation factor Λ accounts for the efficiency with which a mode is launched by a ground-based transmitter. Usually, Λ is normalized to unity for TM mode excitation by a vertical dipole in an idealized waveguide sharply bounded by perfect conductors. Such normalization

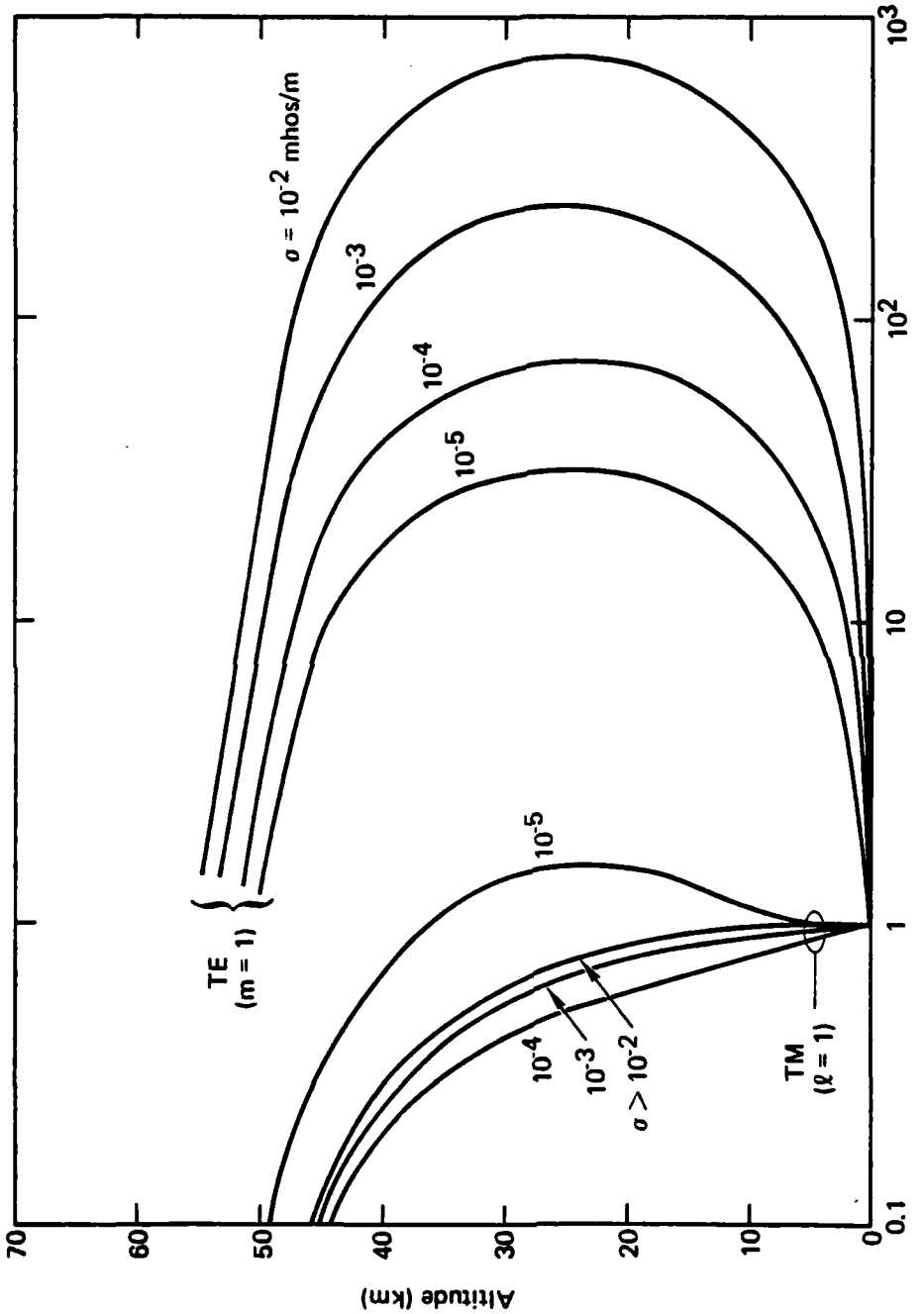

Fig. 3--Height-gain function versus altitude for first TM and TE modes: intense disturbance and f = 20 kHz

is accomplished by factoring out the "height" of the ionosphere, which is well defined in the idealized situation [Galejs, 1972]. However, our diffuse ionospheric models have no well-defined boundary. Consequently, the excitation factors computed here have units of inverse distance, and are smaller than those of other authors (e.g., Wait and Spies [1964]; Galejs [1972]) by a factor roughly corresponding to the average height of the ionospheric region causing the strongest reflections. That is, our excitation factors are defined to include the dependence on the effective width of the waveguide.

Normal Daytime Conditions

Figure 4 shows the frequency dependence of the calculated excitation factor magnitudes A_ℓ and A_m for the first three TM modes (ℓ = 1, 2, 3) and first two TE modes (m = 1, 2) for normal daytime conditions and $\sigma_g = 10^{-3}$ mhos/m. A ground dielectric constant of 10 is assumed throughout. At lower frequencies, multiplying A_ℓ by nominal daytime reflection heights of 6×10^4 to 7×10^4 m gives a result near unity.

The first three TM modes are excited about equally at the lower VLF frequencies, but, above about 30 kHz, the higher order TM modes are more efficiently excited than the first. On the other hand, the TE modes are excited less efficiently than the TM modes. Indeed, A_ℓ exceeds A_m by four or five orders of magnitude. Such behavior prevents ground-based transmitters from radiating TE signals efficiently at low frequencies. Again, the second mode is more effectively excited than the first.

Effects of Ground Conductivity and Ionospheric Disturbances

Figure 5 shows the dependence of the first (m = 1) TE mode's excitation factor on ground conductivity for normal and moderately disturbed conditions. This factor is proportional to $1/\sigma$, provided that $\sigma/\omega\varepsilon\varepsilon_0$ is greater than unity. We noted earlier (from Fig. 3) that the TE height-gain function is proportional to $\sigma^{1/2}$, provided that the terminals are high enough. Therefore, the product $A_m G_m(h_T) G_m(h_R)$ [from

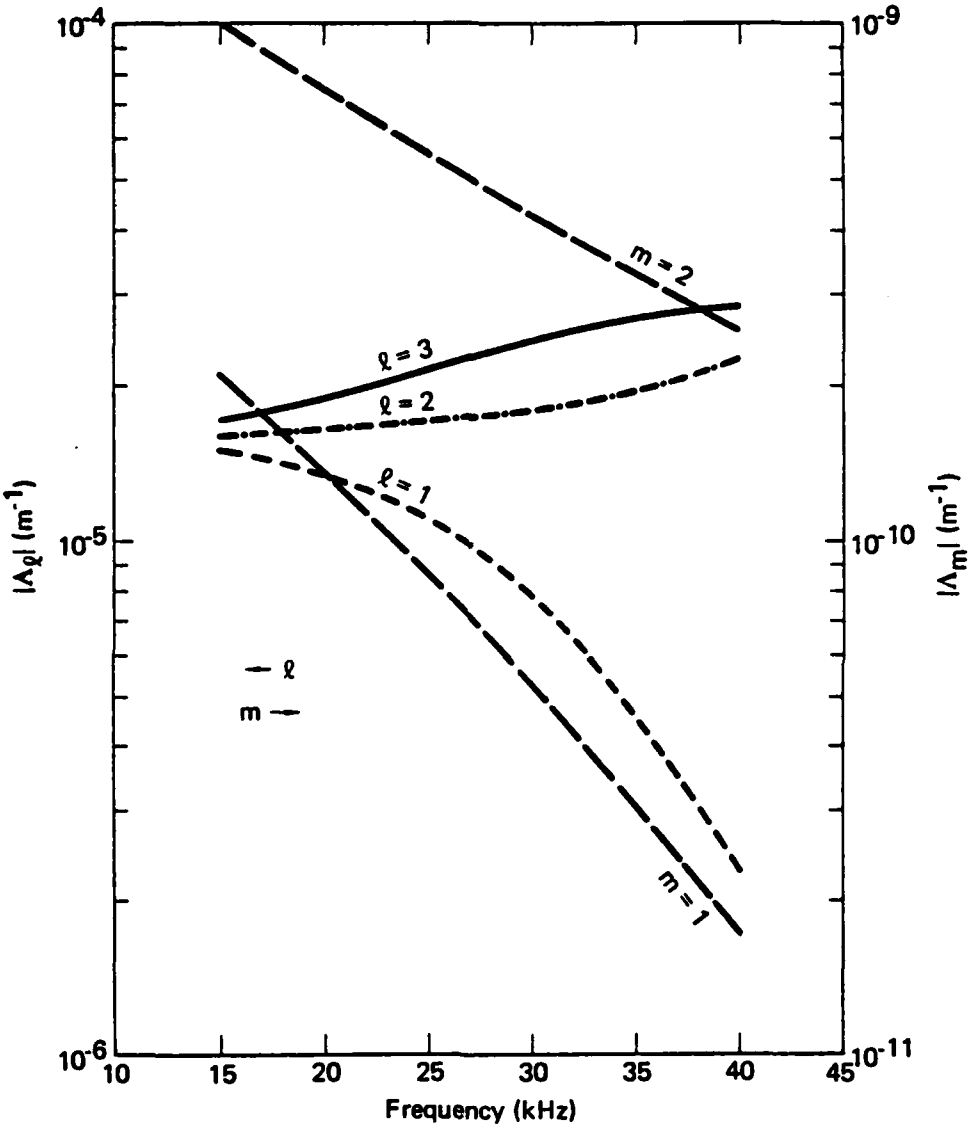

Fig. 4--Excitation factor versus frequency for first three TM modes and first two TE modes: normal daytime conditions and $\sigma = 10^{-3}$ mhos/m

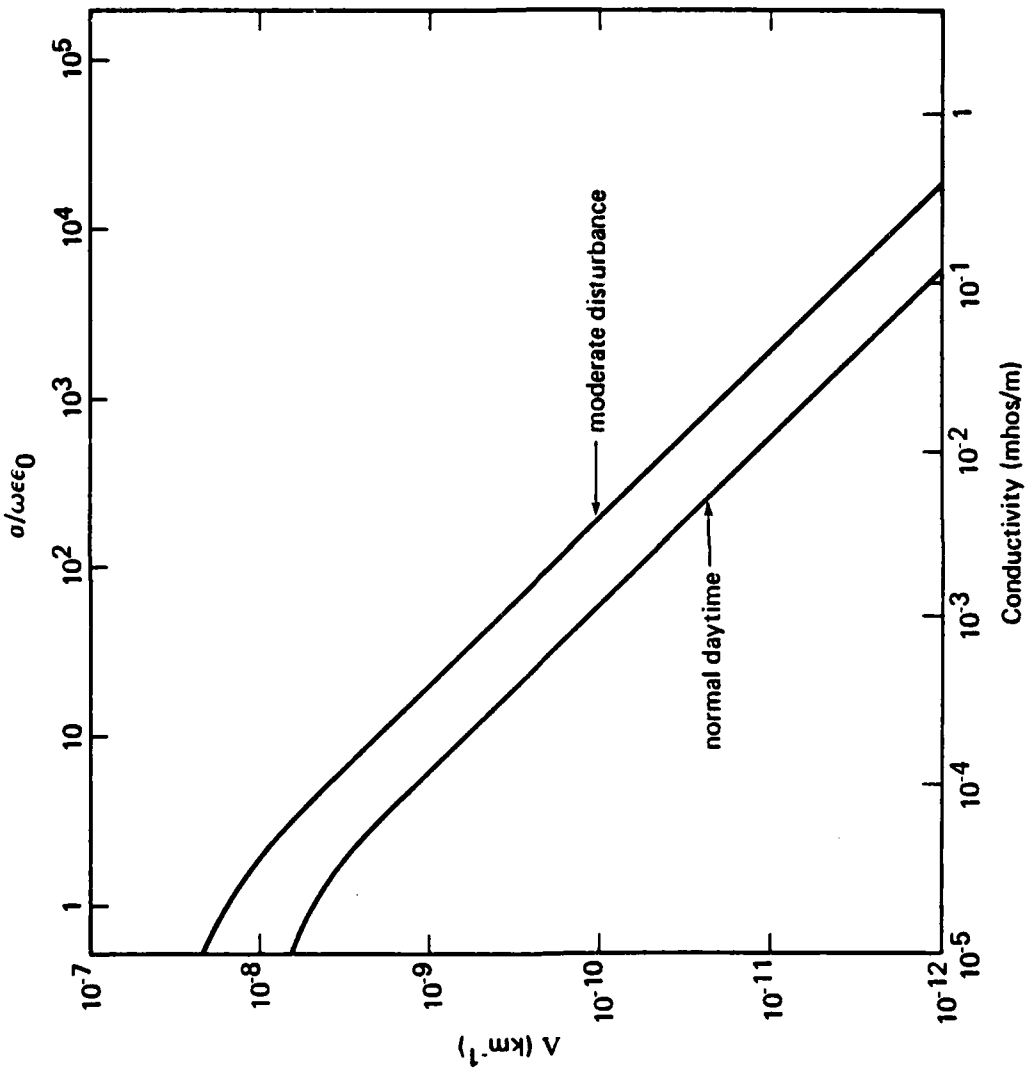

Fig. 5--Excitation factor versus ground conductivity for first TE mode: f = 20 kHz

Eq. (2)] is nearly independent of σ for elevated terminals, even though the individual factors Λ_m and G_m depend strongly on σ.

The above comments indicate that ΛG^2--rather than Λ--is the quantity that accounts for mode excitation. However, for TM modes and typical aircraft altitudes, the height-gain function G is nearly unity and $\Lambda_\ell G_\ell^2 \approx \Lambda_\ell$.

Figures 6 and 7 show how excitation of the lowest TM and TE modes depends on ground conductivity. Figure 6 pertains to a frequency of 20 kHz (representative of TACAMO transmission) and Fig. 7 to a frequency of 35 kHz, which could represent transmissions from any of several airborne transmitters [Kossey et al., 1981]. Both figures compare the excitation under normal and moderately disturbed conditions for terminals elevated 12 km above the ground. As before, we show ΛG^2 for the TE mode, but only Λ for the TM mode.

Several points should be noted from Figs. 6 and 7. First, the disturbance, which constricts the waveguide, increases both TM and TE excitation, since Λ is inversely proportional to waveguide width. Second, the TM mode excitation exhibits a broad maximum for conductivities between, say, 3×10^{-5} and 3×10^{-4} mhos/m. That maximum occurs when the TM eigenangle is near the Brewster's angle of the ground. Third, the TE excitation is nearly independent of conductivity--a consequence of TE signals having no Brewster's angle.

Figures 6 and 7 show that--for a terminal elevation of 12 km--TM excitation is somewhat stronger than TE excitation for most ground conductivities, and much stronger in the Brewster's-angle maximum. However, as shown below (pp. 24-29) TM attenuation becomes prohibitive near the Brewster's angle and destroys the beneficial effects of the enhanced excitation.

The TM excitation curves in Figs. 6 and 7 are valid for all aircraft altitudes, whereas the TE excitation depends strongly on altitude. Figure 8 illustrates that altitude dependence for various ground conductivities. In the usual case, where transmitter and receiver are at different altitudes above different types of ground,

$$E \propto \left[\Lambda^{1/2}(\sigma_T)G(h_T)\right]\left[\Lambda^{1/2}(\sigma_R)G(h_R)\right] \quad , \tag{5}$$

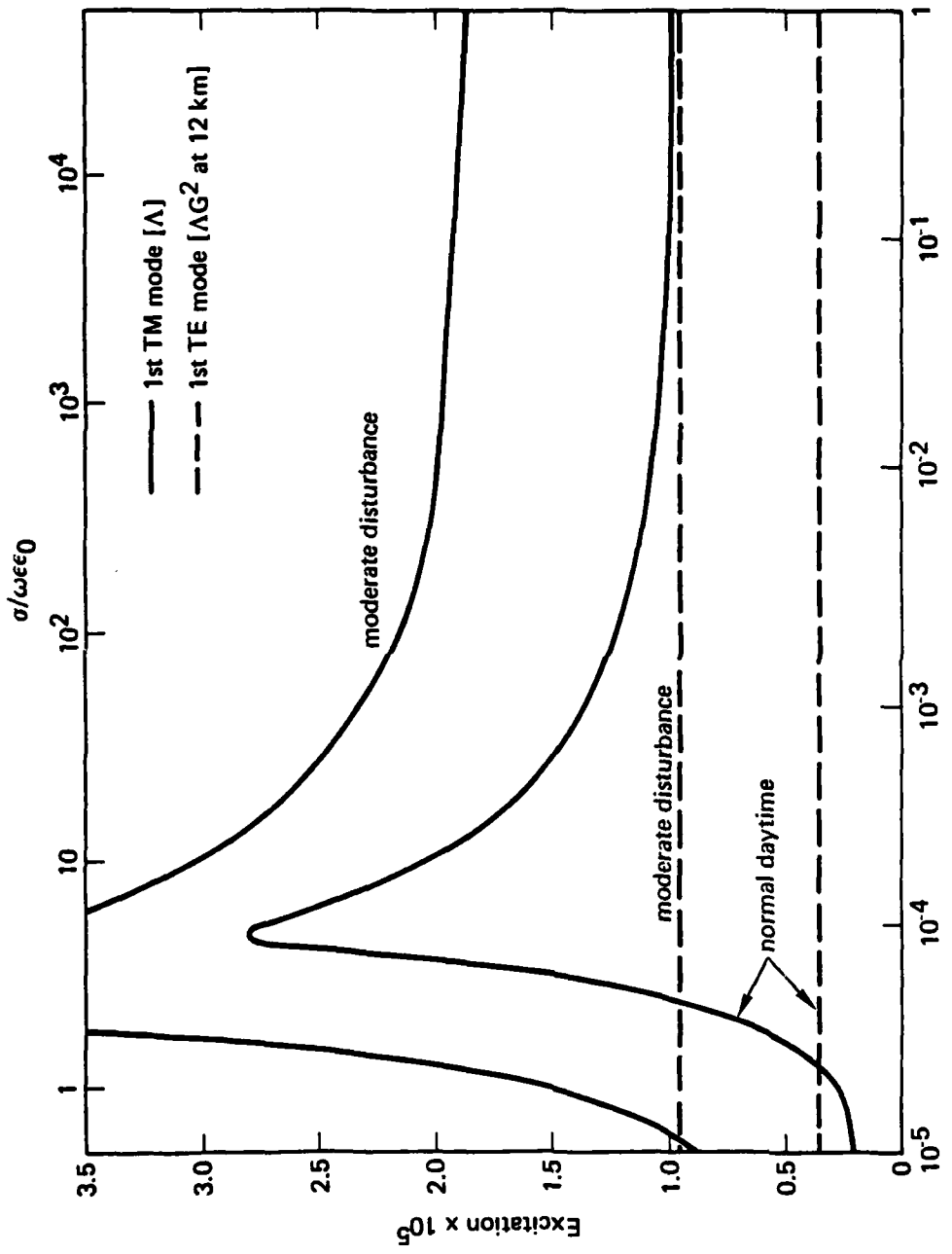

Fig. 6--Excitation of lowest TM and TE modes versus ground conductivity σ for normal daytime and moderately disturbed conditions: f = 20 kHz

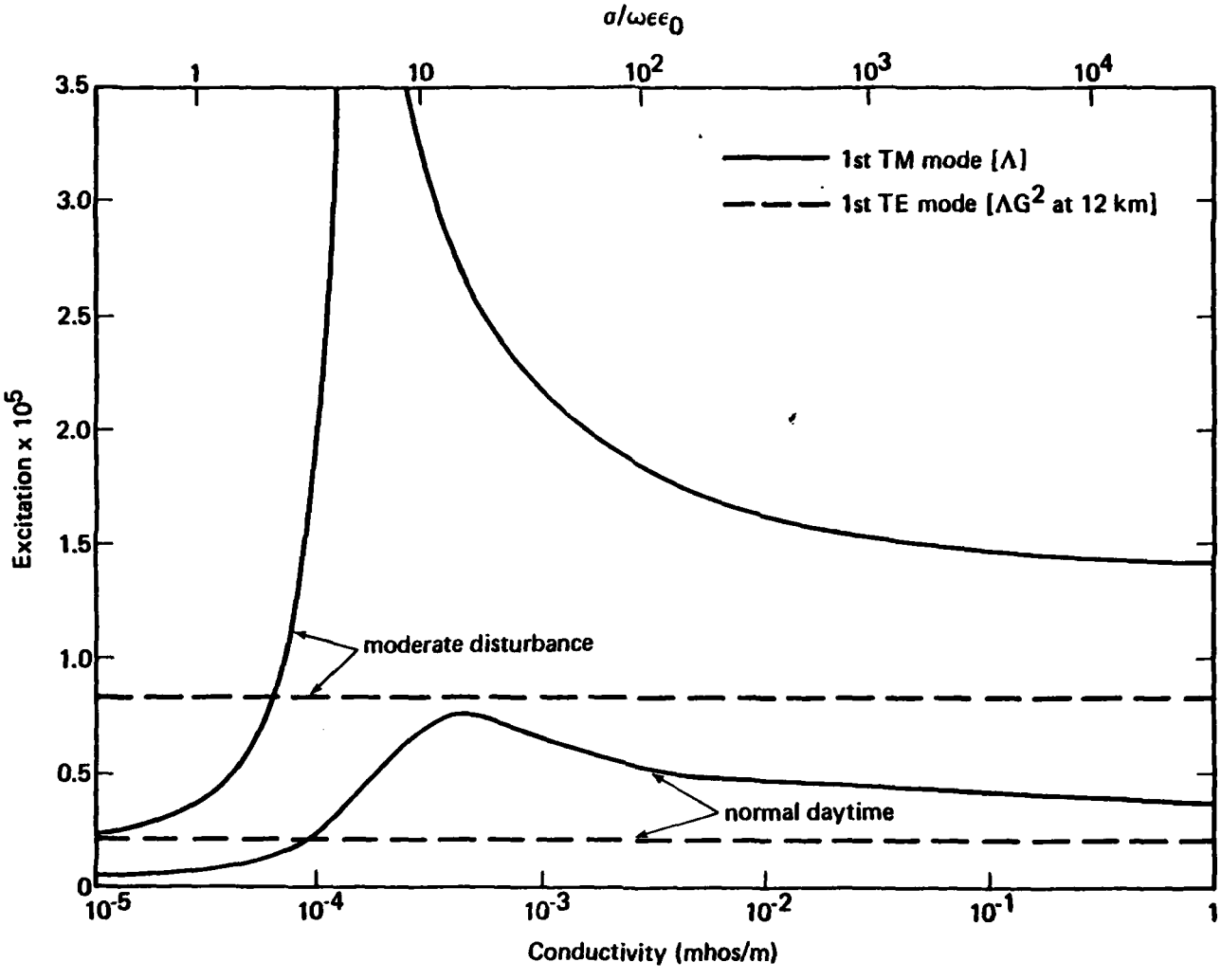

Fig. 7--Excitation of lowest TM and TE modes versus ground conductivity σ for normal daytime and moderately disturbed conditions: f = 35 kHz

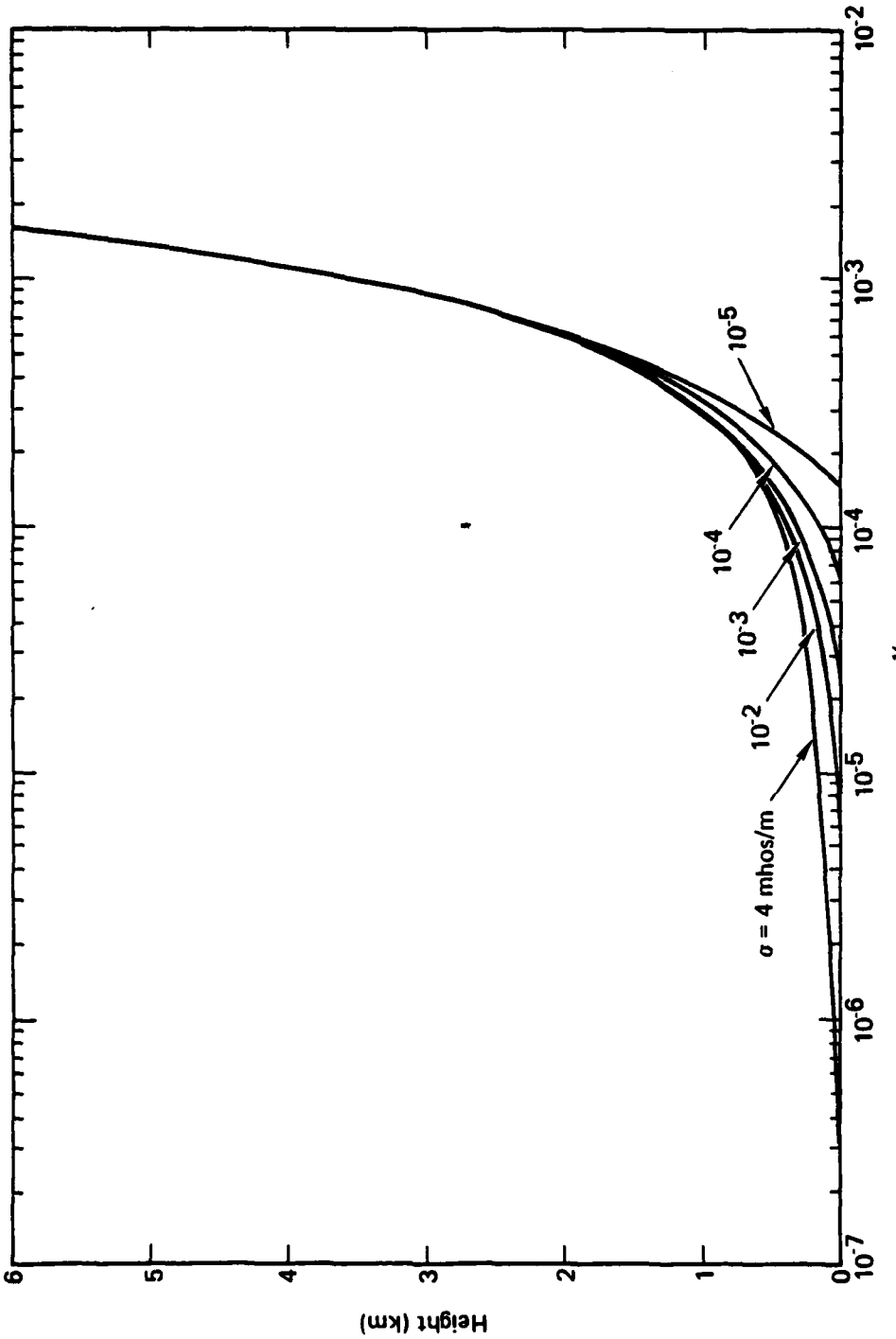

Fig. 8--Excitation of lowest TE mode versus altitude for moderately disturbed conditions: f = 20 kHz

where the subscripts T and R denote quantities at the locations of the transmitter and receiver, respectively. Therefore, to conveniently illustrate the field's dependence on the conductivity and altitude of either terminal, Fig. 8 shows $A^{1/2}G$ for the first TE mode.

The curves in Fig. 8 show that TE excitation becomes independent of ground conductivity σ for aircraft higher than about 1.5 km (~5000 ft), but depends strongly on σ for terminals at lower altitudes. Comparison of Fig. 8 with Fig. 7 shows that TE excitation is extremely weak for ground-based terminals, particularly over well-conducting ground. Although calculated specifically for moderately disturbed conditions, the curves in Fig. 8 are typical of those calculated for other ionospheric conditions as well.

ATTENUATION RATES

Normal Daytime Conditions

Figure 9 plots attenuation rate as a function of frequency for the first three TM modes (ℓ = 1, 2, 3) and the first two TE modes (m = 1, 2) for normal daytime conditions and $\sigma_g = 10^{-3}$ mhos/m. The higher order modes are more heavily attenuated than the lower, which often allows them to be neglected at VLF for long pathlengths. At higher frequencies, the attenuation of higher order modes can be alleviated by efficient excitation (as Fig. 4 shows). It is therefore necessary to retain many terms in the mode sum, as Eqs. (1) and (2) do, throughout the LF band under normal conditions. In that case, geometric optics is often a more convenient approach to propagation analysis than is mode theory.

For intense disturbances the analysis is simpler than that for ambient conditions, since the higher order modes are strongly attenuated and the mode sum can be used well into the LF regime. In fact, a single mode often suffices to describe the signal. Figure 9 shows that the first TE mode is slightly less attenuated than the first TM mode, although that result depends on the specific normal daytime conditions and ground conductivity assumed.

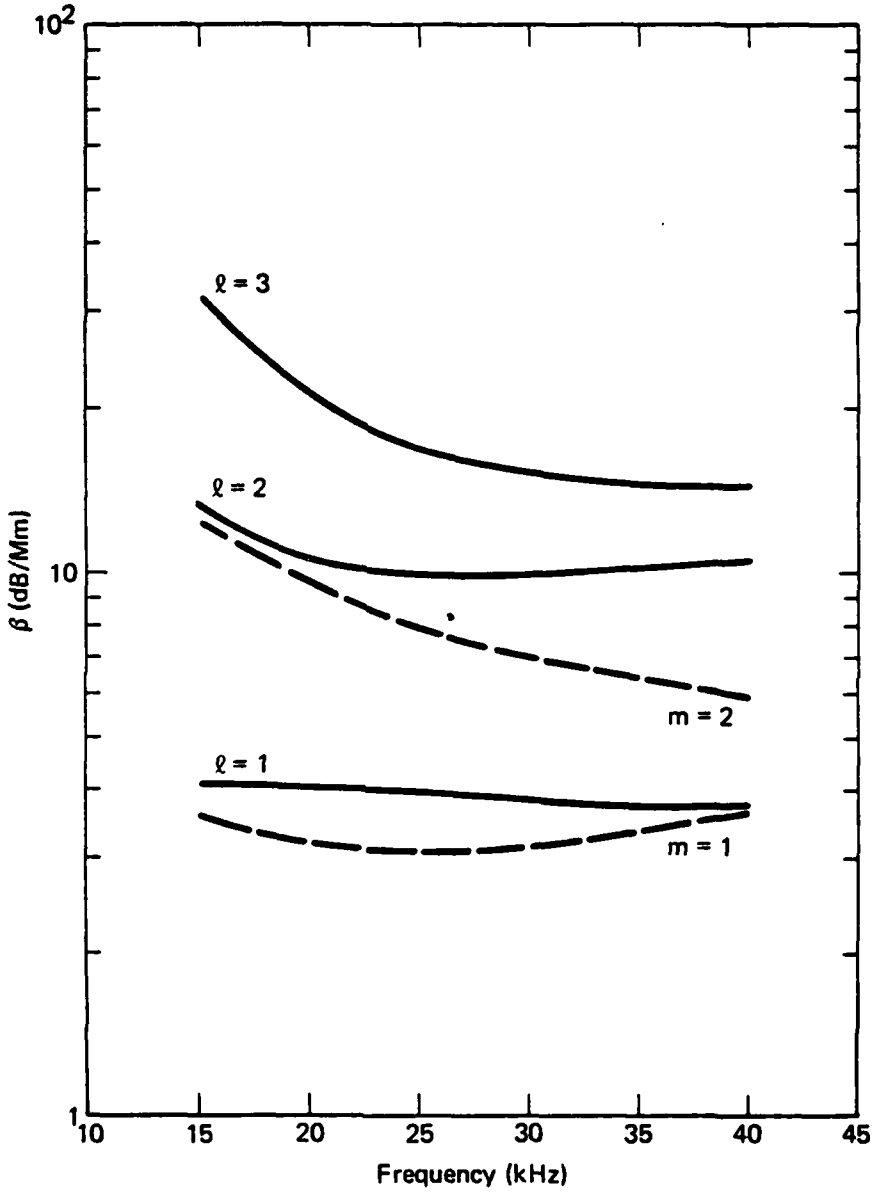

Fig. 9--Attenuation rate β versus frequency f for first three TM modes and first two TE modes: normal daytime conditions and $\sigma = 10^{-3}$ mhos/m

Effects of Ionospheric Disturbances

Figures 10 and 11 show the dependence of the lowest TM and TE modes' attenuation rates on the severity of a disturbance. The curves pertain to several VLF/LF frequencies, and were calculated for the case of perfectly conducting ground. The extreme left sides of Figs. 10 and 11 correspond to the normal daytime model shown in Fig. 1, whereas the extreme right side corresponds to a very intense disturbance. In addition, our calculations employed 12 intermediate levels of disturbance, including the moderate and intense profiles of Fig. 1.

For all levels of disturbance shown in Figs. 10 and 11, the TE mode is more heavily attenuated than the TM mode. The excess TE mode attenuation is plotted in Fig. 12. It is seen to be slight for normal or weakly disturbed conditions, but severe for moderate or intense disturbances.

Although calculated for infinite ground conductivity, the curves shown in Figs. 10 through 12 approximate the attenuation rates if $\sigma > 10^{-3}$ mhos/m. However, we show below that the TM results change drastically if $\sigma < 10^{-3}$ mhos/m.

Dependence on Ground Conductivity

Figures 13 and 14 show the dependence on ground conductivity of the attenuation rates of the first TM and TE modes at 20 and 35 kHz, respectively. Results are given for normal daytime conditions and a moderate disturbance, which could be either an SPE or a spread-debris nuclear environment. The disturbance increases the attenuation rate of both polarizations over normal values. The TE attenuation rate is virtually independent of ground conductivity, whereas the TM rate exhibits a strong, broad maximum for conductivities between 3×10^{-5} and 3×10^{-4} mhos/m. The TM mode propagates somewhat better than the TE mode for the most common ground conductivities, but propagates much worse over low-conductivity ground. The extreme sensitivity of the TM mode to ground conductivity--combined with uncertain parameter values--causes great uncertainty in the calculation of transpolar signals from vertical VLF transmitters, particularly during ionospheric disturbances.

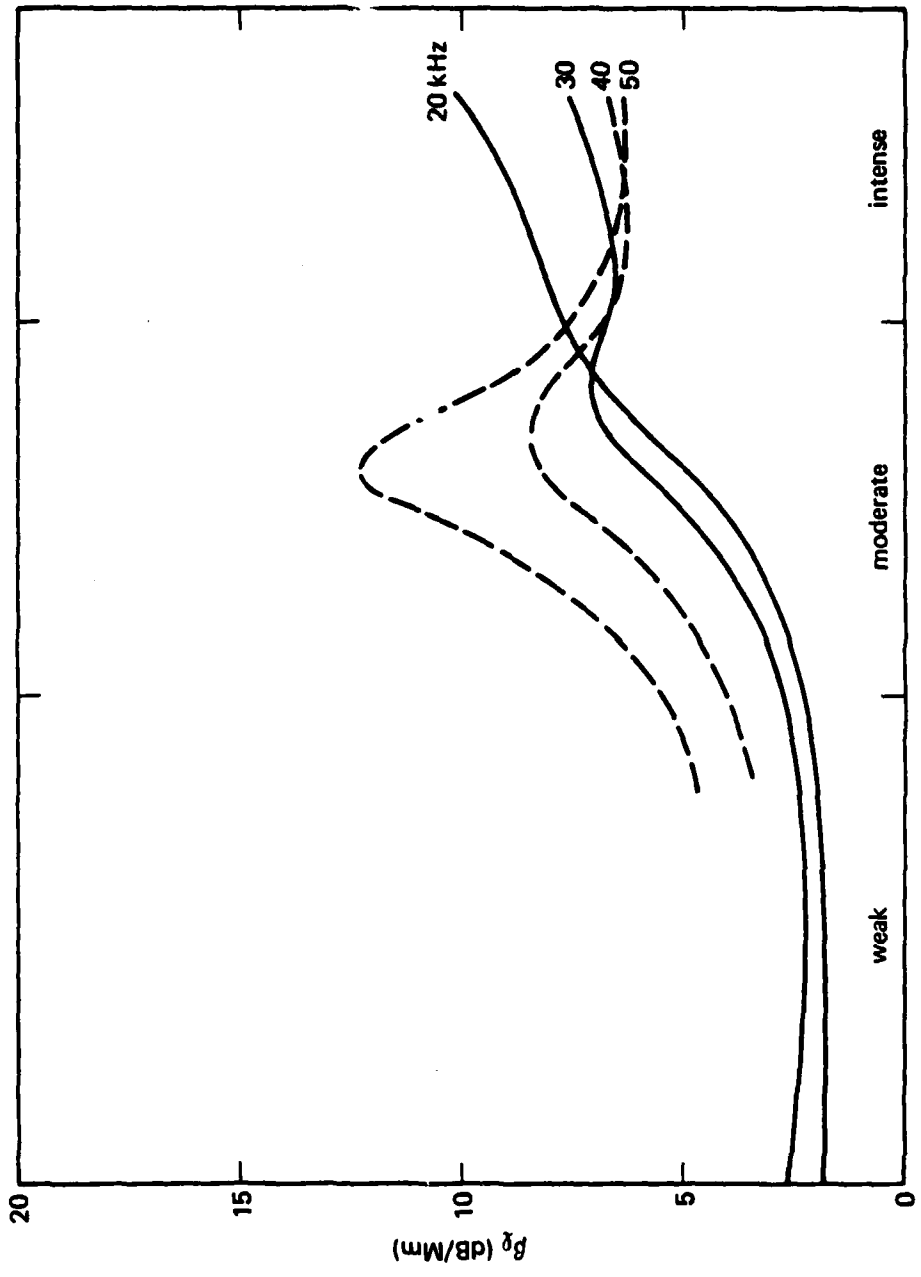

Fig. 10--Attenuation rate β of lowest TM mode: σ = ∞. The severity of the disturbance increases continuously from normal daytime conditions (extreme left) to very intense (extreme right).

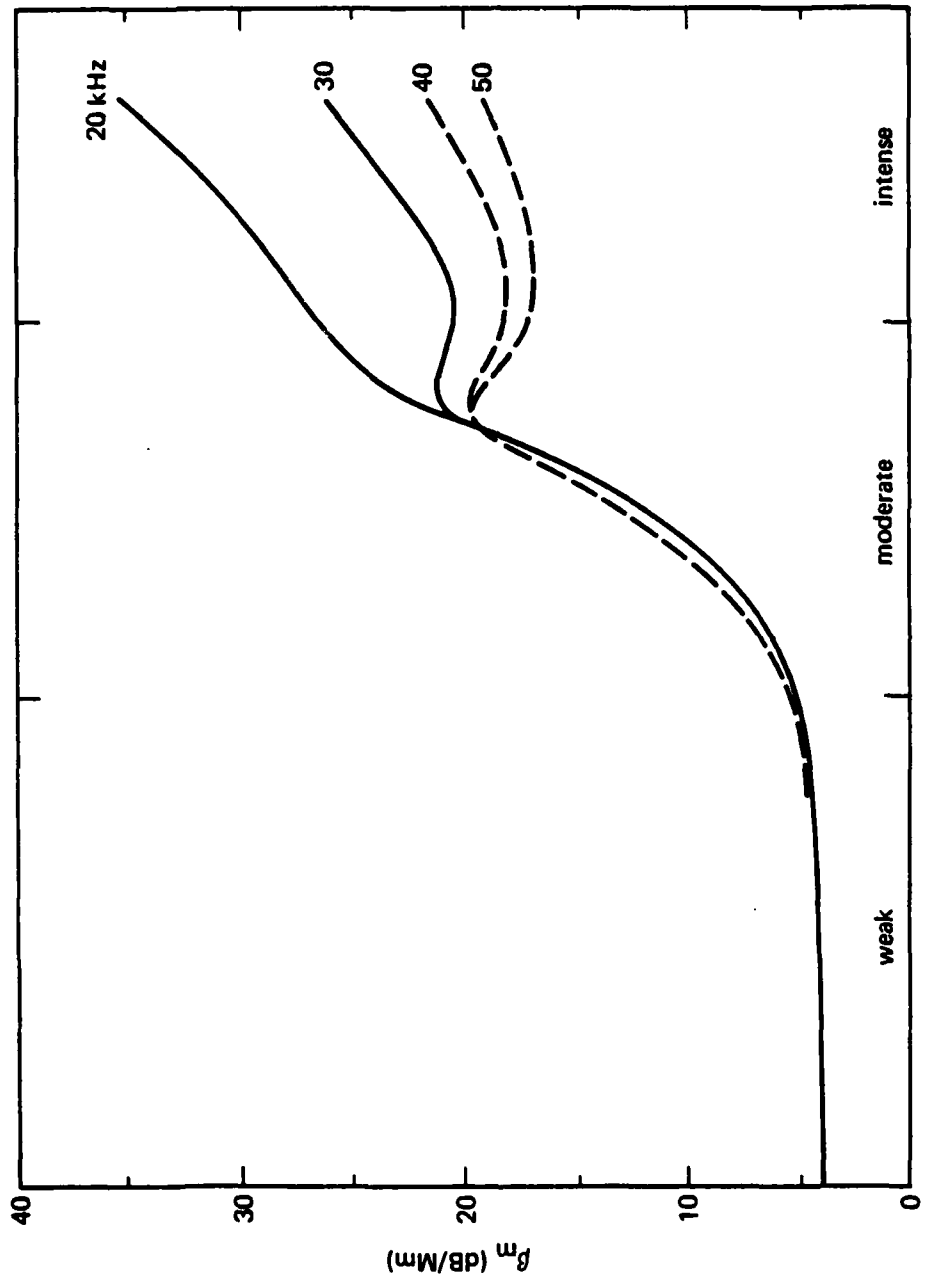

Fig. 11--Attenuation rate β of lowest TE mode: σ = ∞. The severity of the disturbance increases continuously from normal daytime conditions (extreme left) to very intense (extreme right).

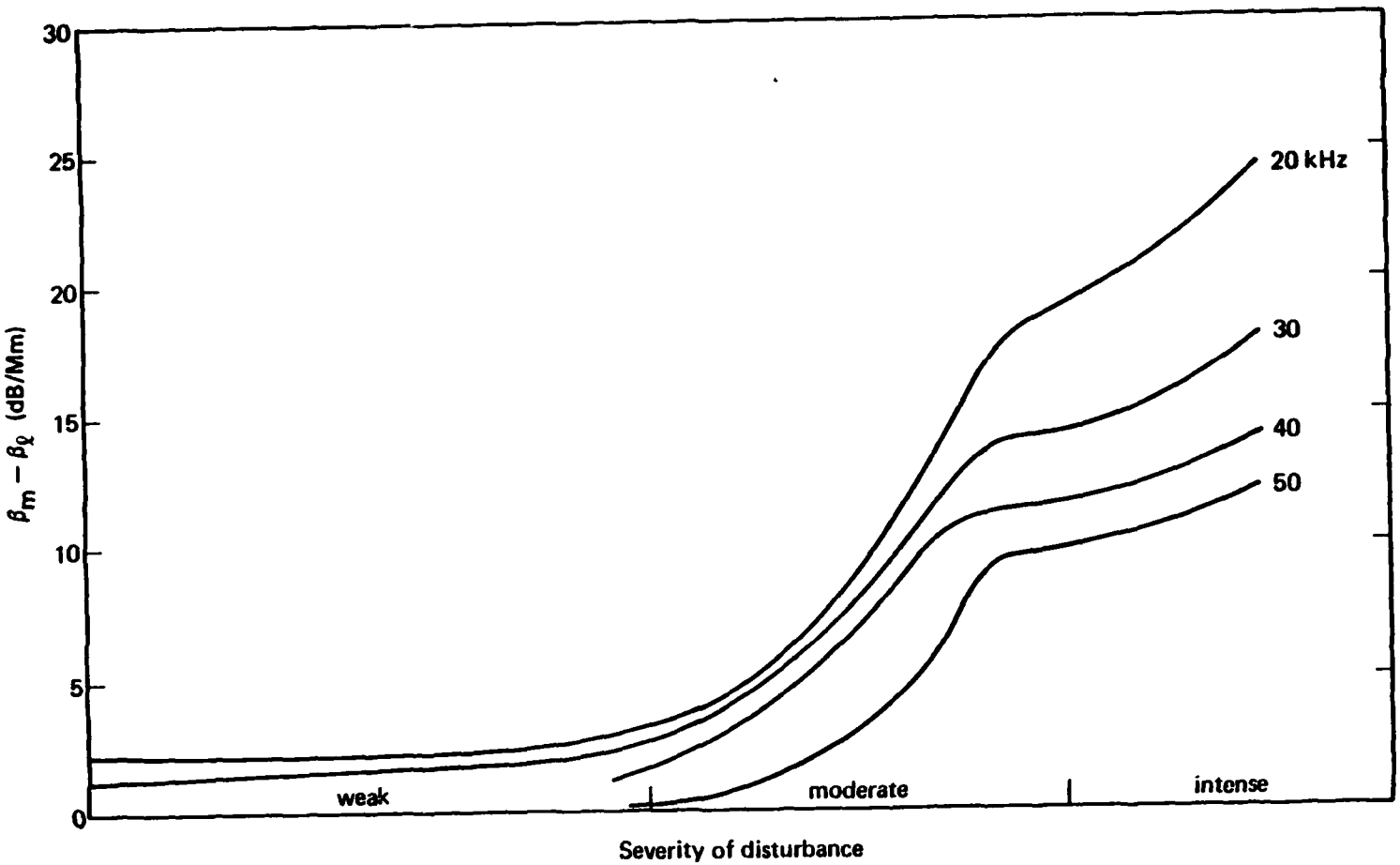

Fig. 12--Amount by which attenuation rate of lowest TE mode exceeds that of lowest TM mode: $\sigma = \infty$. The intensity of the disturbance varies continuously from normal daytime conditions (extreme left) to very intense (extreme right).

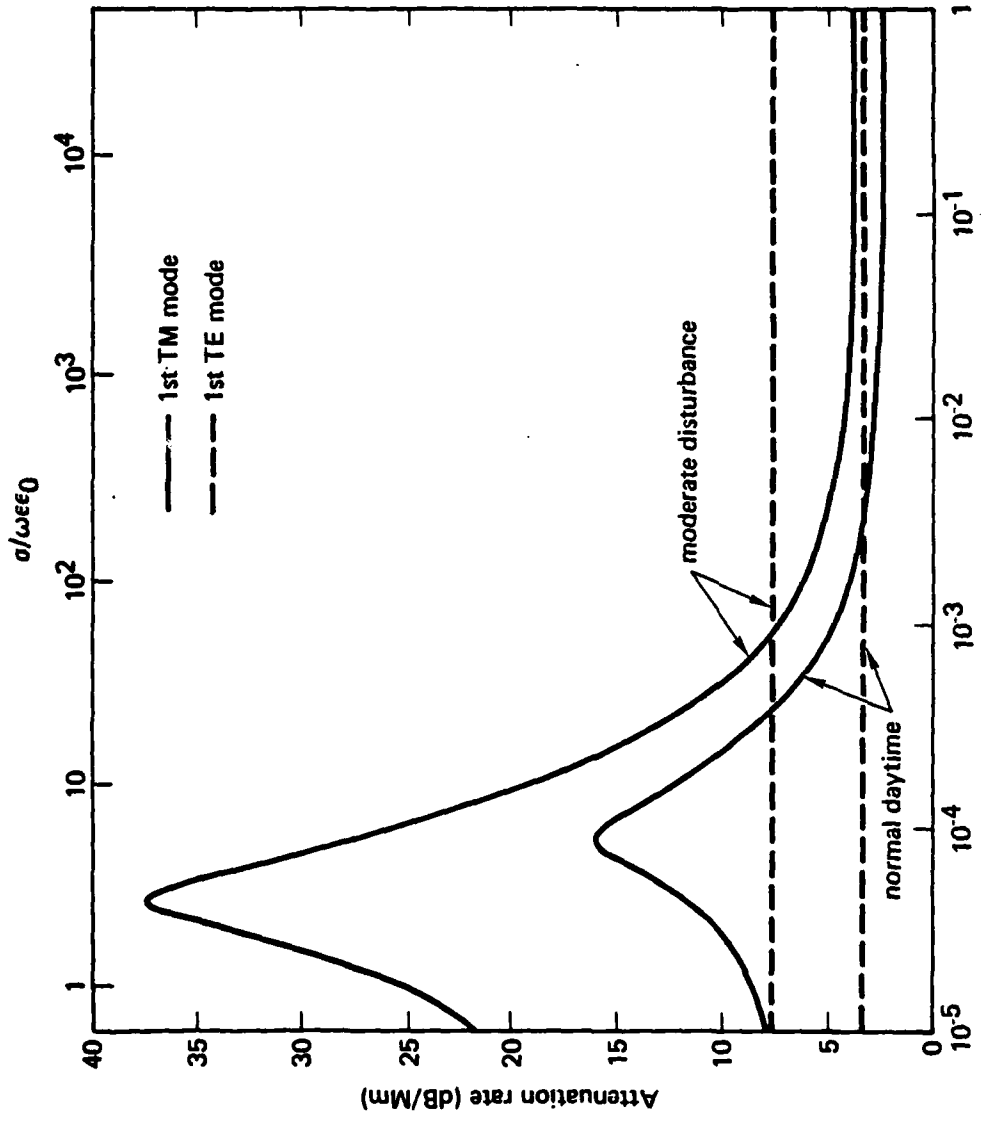

Fig. 13--Attenuation rate β versus ground conductivity σ for normal and moderately disturbed conditions: f = 20 kHz

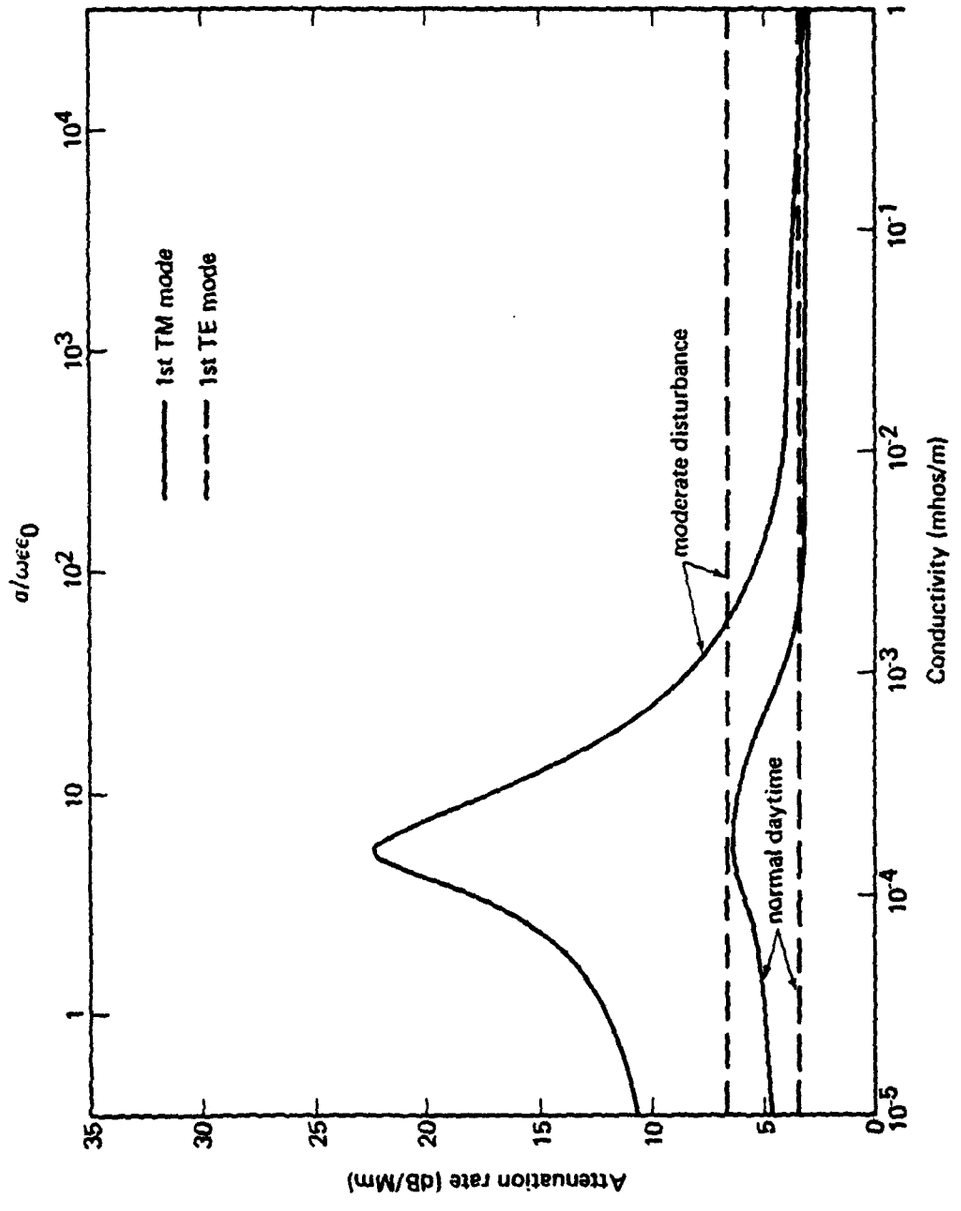

Fig. 14--Attenuation rate β versus ground conductivity σ for normal and moderately disturbed conditions: f = 35 kHz

The main difference between the curves in Figs. 13 and 14 is that the Brewster's-angle peak in the TM attenuation rate is less pronounced at 35 kHz than at 20 kHz. Also, the peak occurs at higher values of σ for the higher frequency.

COMPARISONS OF EXPERIMENT AND THEORY

No experiments have simultaneously measured VLF/LF propagation and ionospheric-conductivity height profiles between 35 and 75 km during a widespread disturbance. We therefore cannot make detailed comparisons between theory and experiment. Nonetheless, many data substantiate the following three theoretically predicted TM mode phenomena: (1) an intense, widespread ionospheric disturbance will significantly degrade long-path VLF signals; (2) poorly conducting ground causes considerable TM signal loss; and (3) an ionospheric disturbance degrades TM signals more severely on paths over poorly conducting ground than over seawater.

Oelberman et al. [1969] measured SPE effects on VLF propagation, and found that the Seattle-to-Switzerland signal typically decreased 10 to 20 dB during such an event. Westerlund and his colleagues [1969, 1973] found that VLF signals propagating across Greenland are sharply degraded by the poorly conducting ice. Moreover, their data showed that SPEs cause much greater signal loss on paths that cross Greenland than on paths over seawater.

Field, Greifinger, and Schwartz [1972] compared calculations with data from a laboratory model that simulated VLF TM propagation in the earth-ionosphere waveguide. Both calculations and data showed that (1) lowering the waveguide's upper boundary increased the signal's attenuation, (2) severe attenuation occurred over a simulated ice cap, and (3) lowering the waveguide boundary caused much greater signal loss over the simulated ice cap than over simulated seawater. Mode-coupling at the seawater/ice-cap boundary was noted in the data but not included in the calculations.

The above data pertain solely to TM signals from ground-based vertical transmitters. To our knowledge, no data exist for long-range TE signals propagating through disturbed regions or over the ice cap.

However, the Rome Air Development Center has made TE measurements of 20 kHz TACAMO transmissions under normal conditions [Kossey et al., 1981]. These signals--radiated from a nearly horizontal trailing-wire antenna--exhibited height-gain functions that closely resembled those shown in Fig. 2 for the entire width of the earth-ionosphere waveguide. Moreover, measurements of a 40 kHz signal from a trailing-wire antenna on an aircraft at 30,000 ft altitude showed that the TE signal exceeded the TM signal at distances up to 1 Mm (where measurements were terminated) and filled spatial nulls exhibited by the TM signal.

V. DISCUSSION

This section describes, quantitatively, the most relevant features of TE and TM signals propagating between airborne terminals, using the results of Sec. IV.

EXCITATION EFFICIENCY

We begin by comparing the amplitude of the TE and TM fields radiated by an inclined trailing-wire antenna. Equations (1) and (2) show that, for long propagation paths where a single mode adequately represents the signal, the ratio of the broadside TE to TM field strengths is

$$\left|\frac{E_H}{E_V}\right| \simeq \tan\psi \, \frac{\Lambda_m G_m^2(h)}{\Lambda_\ell} \exp\left[-\frac{(\beta_m - \beta_\ell)d}{8.7}\right]\Bigg|_{\ell,m=1} , \tag{6}$$

where $h_T = h_R = h$, $S \approx 1$, and, at aircraft altitudes, $G_{\ell=1} \approx 1$.

The exponential term in Eq. (6) accounts for propagation. We define the other terms to be the relative excitation efficiency, which is given by

$$\mathcal{E}_R \equiv \tan\psi \, \frac{\Lambda_m G_m^2(h)}{\Lambda_\ell}\Bigg|_{m,\ell=1} . \tag{7}$$

The quantity $\mathcal{E}_R$ denotes the ratio of the broadside excitation efficiency of the lowest TE mode to that of the lowest TM mode. Equation (7) shows that $\mathcal{E}_R$ is proportional to the tangent of the inclination angle of the transmitting antenna. It is infinite for horizontal ($\psi = 90°$) antennas and zero for vertical ($\psi = 0°$) ones.

Figures 6 and 7 show that, for high-flying aircraft over typical ground, the quantity $\Lambda_m G_m^2/\Lambda_\ell$ has a magnitude of approximately 0.5. Thus, an antenna having equal vertical and horizontal components

(ψ = 45°) would excite a TE component several decibels weaker than the TM component. However, ψ attains values of 75 to 80 deg for high-speed aircraft, and tan ψ lies between 3.75 and 5.75. Under such conditions, the TE component is several decibels stronger than the TM. That conclusion is borne out by TE/TM measurements made on LF signals radiated by high-speed aircraft (e.g., Kossey et al. [1981]).

The above points apply to aircraft at altitudes between 35,000 and 40,000 ft. For lower altitudes, the TE signal becomes weaker (Fig. 8), whereas the TM signal remains nearly constant. The quantity $\mathcal{E}_R$ exceeds unity for high-speed aircraft if the altitude exceeds about 20,000 ft.

Figures 6 and 7 show that the TM signal is more strongly excited than the TE signal if ground conductivity is between 3×10^{-5} and 3×10^{-4} mhos/m. However, Figs. 13 and 14 show that the TM attenuation rate also exhibits a strong Brewster's-angle peak at those conductivities. As discussed below, such a peak attenuation destroys the benefits of the enhanced excitation, except for very short propagation paths.

ATTENUATION

The difference in propagation loss between the lowest TE and TM modes is

$$\Delta TL = -\left[\beta_{m=1} - \beta_{\ell=1}\right] d \quad dB \ . \tag{8}$$

Figures 13 and 14 show that the difference between the attenuation rates of the first TE and TM modes is slight for normal daytime and typical ground conductivities. Under such circumstances, ΔTL is small and, therefore, the excitation efficiency governs the relative magnitudes of TE and TM signals out to considerable ranges. However, the TE and TM attenuation rates differ substantially either under disturbed conditions or during propagation over poorly conducting ground. In those two circumstances, the relative magnitudes of the fields depend more strongly on propagation loss than on excitation.

Figure 13 shows that for a frequency of 20 kHz and poor ground conductivity, $\beta_{\ell=1}$ can exceed $\beta_{m=1}$ by more than 10 dB/Mm. It follows from Eq. (8) that the propagation loss suffered by the TM signal will exceed that suffered by the TE signal by several tens of decibels for pathlengths of a few megameters. Such excess attenuation destroys the advantage in excitation enjoyed by the TM signal for propagation near the Brewster's angle. Figure 14 shows that this effect is present--although less pronounced--in the LF band. Thus, TE signals appear better suited for VLF air-to-air links over areas of poorly conducting ground, such as exists throughout Greenland and much of Canada.

Figure 12 shows that moderate-to-intense ionospheric disturbances can cause $\beta_{m=1}$ to exceed $\beta_{\ell=1}$ by 10 to 25 dB/Mm at VLF, and 5 to 15 dB/Mm at LF. Under such circumstances, ΔTL will be negative and have a magnitude of several tens of decibels for long paths. TE signals are therefore less well suited than TM signals for long-range propagation under moderately or severely disturbed ionospheric conditions.

PROTECTION AGAINST GROUND-BASED JAMMER

Figure 3 shows that strong ionospheric disturbances cause the fields to be confined to altitudes below 60 km, where frequent collisions between charged and neutral particles almost totally suppress geomagnetic effects. Under such conditions, a vertical antenna excites no usable TE signal, and jamming must be accomplished with horizontal antennas.

It can be shown from Eq. (5) that a high-altitude airborne transmitter achieves the following advantage, AJ, over a TE jammer:

$$AJ = 20 \log_{10} \left[\frac{\Lambda_m^{1/2}(\sigma_T) G_m(\sigma_T, h_T)}{\Lambda_m^{1/2}(\sigma_J) G_m(\sigma_J, h_J)} \right]_{m=1} \quad \text{dB} , \tag{9}$$

where the subscript J denotes parameters pertaining to the location of the jammer. Figure 8 shows that $\Lambda^{1/2}G$ is independent of conductivity if the terminal is higher than about 1.5 km, whereas the

height-gain function G is unity if h = 0. Therefore, when a high-altitude transmitter is countered by a ground-based jammer, Eq. (9) can be rewritten in the simpler form

$$AJ = 20 \log_{10}\left[\frac{\Lambda_m^{1/2} G_m(h_T)}{\Lambda_m^{1/2}(\sigma_J)}\right] \quad dB , \tag{10}$$

which depends only on the transmitter altitude and the ground conductivity at the jammer.

Numerical values for AJ can be obtained directly from Fig. 8 by noting that G = 1 for h = 0. For the usual case where ground conductivity exceeds 10^{-3} mhos/m, a transmitter above 20,000 ft would have at least a 40 dB advantage over a ground-based jammer. That advantage is reduced to about 30 dB if $\sigma_J = 10^{-4}$ mhos/m and to about 20 dB if $\sigma_J = 10^{-5}$ mhos/m. However, such low conductivities are unlikely to occur at optimum locations for ground-based enemy jammers.

The signal-to-jammer ratio is independent of receiver height, because both the communication and jamming signals have the same altitude dependence at long ranges. At short ranges, the signal-to-jammer ratio has a complicated height dependence because of many contributing waveguide modes.

The above discussion concerns only disturbed conditions, where geomagnetic conversion is negligible. Calculations and measurements have shown that, during normal daytime, geomagnetic conversion can cause a vertical antenna to excite an elliptically polarized signal with a horizontal component 20 percent as strong as the vertical component [Kossey, 1981; Moler, 1980]. Such conversion of vertical-to-horizontal polarization is even stronger during normal nighttime. Therefore, under normal conditions, a powerful, vertically polarized, ground-based jammer could degrade the performance of an air-to-air TE link, although less seriously than it could a comparable TM link.

SIGNAL-TO-NOISE RATIO OF TE LINKS

Thus far we have addressed the behavior of TE and TM signals under various conditions. However, signal-to-noise ratio (SNR), rather than signal strength alone, governs the performance of a communication link. Accordingly, we now describe the dependence of the TE SNR on the altitudes of the terminals.

It follows from Eq. (5) that

$$\mathrm{SNR} \propto \left. \frac{\left[\Lambda_m^{1/2} G(h_T)\right]\left[\Lambda_m^{1/2} G(h_R)\right]}{N_a + N_T + N_P} \right|_{m=1} \tag{11}$$

for TE air-to-air links, where N_a, N_T, and N_P denote atmospheric, platform, and receiver noise, respectively. The variation of SNR with receiver altitude depends on whether the link is system-noise-limited ($N_T + N_P \gg N_a$) or atmospheric-noise-limited ($N_a \gg N_T + N_P$). The relative importance of the three types of noise depends on the type of aircraft, the location of the receiver on the aircraft, and the degree of platform-noise suppression achieved.

If the link is system-noise-limited, the denominator in Eq. (11) is nearly independent of altitude, and the SNR has the same altitude dependence as the signal [see Eq. (5)]. If the link is atmospheric-noise-limited, Eq. (11) becomes approximately

$$\mathrm{SNR} \propto \left. \frac{\left[\Lambda_m^{1/2} G_m(h_T)\right]\left[\Lambda_m^{1/2} G_m(h_R)\right]}{N_a} \right|_{m=1} . \tag{12}$$

Atmospheric noise propagates from distant thunderstorms* in the earth-ionosphere waveguide, in much the same manner as a signal. Therefore, the altitude dependence of pure TE noise is governed by the height-gain function of the dominant waveguide modes.

*Impulsive noise from nearby thunderstorms can be removed by using nonlinear processing, such as clipping.

For long-path single-mode propagation, such dependence is given by

$$N_a \propto \left[\Lambda_m^{1/2} G_m(h_R)\right]_{m=1} , \tag{13}$$

which, when combined with Eq. (12), gives

$$\text{SNR} \propto \left[\Lambda_m^{1/2} G_m(h_T)\right]_{m=1} , \qquad \text{if } N_a >> N_P + N_T . \tag{14}$$

Equation (14) shows that SNR depends on transmitter altitude--but not receiver altitude--in an atmospheric-noise-limited situation. Independence of receiver altitude is typical of atmospheric-noise-limited links. A well-known example is a submerged receiver, where the SNR is independent of depth because signal and noise are equally attenuated by seawater.

The above discussion applies only when geomagnetic conversion is unimportant, and TE modes can exist independently of TM modes. Otherwise, geomagnetically converted TM noise must be accounted for.

REFERENCES

Field, E. C., C. Greifinger, and K. Schwartz, "Transpolar Propagation of Long Radio Waves," *J. Geophys. Res.*, Vol. 77, No. 7, March 1972, pp. 1264-1278.

Field, E. C., *VLF/LF TE-Mode Propagation under Disturbed Ionospheric Conditions*, Air Force Cambridge Research Laboratory, AFCRL-TR-75-0382, July 1975.

Field, E. C., et al., *Effects of Antenna Elevation and Inclination on VLF/LF Signal Structure*, Air Force Systems Command, Rome Air Development Center, RADC-TR-76-C-375, December 1976.

Galejs, J., *Terrestrial Propagation of Long Electromagnetic Waves*, Pergamon Press, New York, 1972.

Kossey, P. A., Rome Air Development Center, Hanscom Air Force Base, Mass., private communication, 1981.

Kossey, P. A., et al., "Relative Characteristics of TE/TM Waves Excited by Airborne VLF/LF Transmitters," presented at the Electromagnetic Wave Propagation Panel of NATO/AGARD, Brussels, Belgium, 21-25 September 1981 (available through the National Technical Information Service, Springfield, Virginia).

Lewis, E. A., and R. P. Harrison, *Experimental Evidence of a Strong TE-Polarized Wave from an Airborne LF Transmitter*, Air Force Cambridge Research Laboratory, AFCRL-TR-75-0555, October 1975.

Moler, W., Naval Ocean Systems Center, San Diego, Calif., private communication, 1980.

Oelberman, E. J., et al., *Coordinated High-Latitude Experiments for the Simulation of Nuclear Burst Effects on VLF Systems*, HRB-Singer, State College, Pennsylvania, Report 336-F, February 1969.

Pappert, R. A., "Effects of Elevation and Ground Conductivity on Horizontal Dipole Excitation of the Earth-Ionosphere Waveguide," *Radio Sci.*, Vol. 5, March 1970, pp. 579-590.

Pappert, R. A., and W. F. Moler, "Propagation Theory and Calculations at Lower Extremely Low Frequencies (ELF)," *IEEE Trans. Comm.*, Vol. COM-22, April 1974, pp. 438-451.

Wait, J. R., *Electromagnetic Waves in Stratified Media*, Pergamon Press, New York, 1970.

Wait, J. R., and K. P. Spies, *Characteristics of the Earth-Ionosphere Waveguide for VLF Radio Waves*, U.S. Department of Commerce, National Bureau of Standards, Washington, D.C., Technical Note 300, 1964.

Westerlund, S., and F. H. Reider, "VLF Radio Signals Propagating over the Greenland Ice-Sheet," *J. Atmos. Terr. Phys.*, Vol. 35, 1973, pp. 1475-1491.

Westerlund, S., et al., "Effects of Polar Cap Absorption Events on VLF Transmissions," *Planet. Space Sci.*, Vol. 17, 1969, pp. 1329-1374.

DISTRIBUTION LIST

Department of Defense

Director
Defense Advanced Research Projects Agency
1400 Wilson Boulevard
Arlington, Virginia 22209

Attn:	TIO	1
	STO	1
	NRMO	1

Director
Defense Communications Agency
8th Street and South Courthouse Road
Arlington, Virginia 22204

Attn:	MEECN Office	3

Defense Technical Information Center
Cameron Station
Alexandria, Virginia 22314

Attn:	TC	12

Director
Defense Nuclear Agency
Washington, D.C. 20305

Attn:	STTL	1
	DDST	1
	RAAE	3
	RAEV	1

Joint Chiefs of Staff
Department of Defense
Washington, D.C. 20301

Attn:	J-6	1

Director
National Security Agency
Fort George G. Meade, Maryland 20755

Attn:	Technical Library	2

Under Secretary of Defense (Research and Engineering)
Department of Defense
Washington, D.C. 20301

Attn:	DDS&SS	2

Department of Defense (cont.)

Defense Logistics Agency
DCASMA-Los Angeles
9920 So. La Cienega Boulevard
Inglewood, California 90301
Attn: DCRL-GLCC(L3) 1
Ben Miller

Department of Commerce

U.S. Department of Commerce
Office of Telecommunications
Institute for Telecommunication Sciences
National Telecommunications and Information Administration
Boulder, Colorado 80303
Attn: W. F. Utlaut 2

Department of the Army

Commander/Director
Atmospheric Sciences Laboratory
U.S. Army Electronics Command
White Sands Missile Range, New Mexico 88002
Attn: DRSEL-BL-SY-S 1
F. E. Niles

Director
U.S. Army Ballistic Research Laboratories
Aberdeen Proving Grounds, Maryland 21005
Attn: George E. Keller 1

Commander
U.S. Army Foreign Sciences and Technology Center
220 7th Street, N.E.
Charlottesville, Virginia 22901
Attn: Robert Jones 1

Department of the Navy

Chief of Naval Operations
Department of the Navy
Washington, D.C. 20350
Attn: NOP 985 1
NOP 094H 1
NOP 941 1

Chief of Naval Research
Department of the Navy
800 North Quincy Street
Arlington, Virginia 22217
Attn: Code 414, R. G. Joiner 1

Department of the Navy (cont.)

Commander
Naval Electronic Systems Command
Department of the Navy
Washington, D.C. 20360

Attn:	PME-110	1
	PME-110T	1
	PME-110-X1	1
	PME 110-112	1

Director
Naval Ocean Systems Center
Electromagnetic Propagation Division
271 Catalina Boulevard
San Diego, California 92152

Attn:	Code 2200, W. F. Moler	1
	Code 2200, John Bickel	1

Director
Naval Research Laboratory
4555 Overlook Avenue, S.W.
Washington, D.C. 20375

Attn:	Code 7700, Timothy P. Coffee	1
	Code 7709, Wahab Ali	1
	Code 7750, John Davis	2
	Code 2627	6

Commander
Naval Surface Weapons Center (White Oak)
Silver Spring, Maryland 20910

Attn:	Technical Library	1

Office of Naval Research 1
Pasadena Detachment
1030 East Green Street
Pasadena, California 91106

Department of the Air Force

Commander
Air Force Geophysical Laboratory, AFSC
L. G. Hanscom Air Force Base, Massachusetts 01731

Attn:	OPR	1
	LKB, W. Swider	1
	LKB, K. Champion	1

Director
Air Force Technical Applications Center
Patrick Air Force Base, Florida 32920

Attn:	TD	1
	HQ 1035th TCHOG/TFS	1

Department of Defense Contractors

General Electric Company
TEMPO--Center for Advanced Studies
816 State Street
Santa Barbara, California 93102
Attn: Warren S. Knapp 1
DASIAC 1

Lockheed Missiles and Space Company
3251 Hanover Street
Palo Alto, California 94304
Attn: J. B. Reagan 1
W. Imhof 1
Martin Walt 1

Mission Research Corporation
735 State Street
Santa Barbara, California 93101
Attn: M. Scheibe 1
D. Sowle 1

Pennsylvania State University
Ionospheric Research Laboratory
College of Engineering
318 Electrical Engineering--East Wing
University Park, Pennsylvania 16802
Attn: John S. Nisbet 1
Les Hale 1
A. J. Ferraro 1
H. S. Lee 1

R & D Associates
4640 Admiralty Way
Marina Del Rey, California 90291
Attn: R. Lelevier 1
F. Gilmore 1
R. Turco 1

The Rand Corporation
1700 Main Street
Santa Monica, California 90406
Attn: Cullen Crain 1

Professor Chalmers F. Sechrist 1
155 Electrical Engineering Building
University of Illinois
Urbana, Illinois 61801

Department of Defense Contractors (cont.)

Stanford Research Institute
333 Ravenswood Avenue
Menlo Park, California 94025
Attn: Allen M. Peterson 1
Ray L. Leadabrand 1

Pacific-Sierra Research Corporation
1456 Cloverfield Boulevard
Santa Monica, California 90404
Attn: E. C. Field, Jr. 1

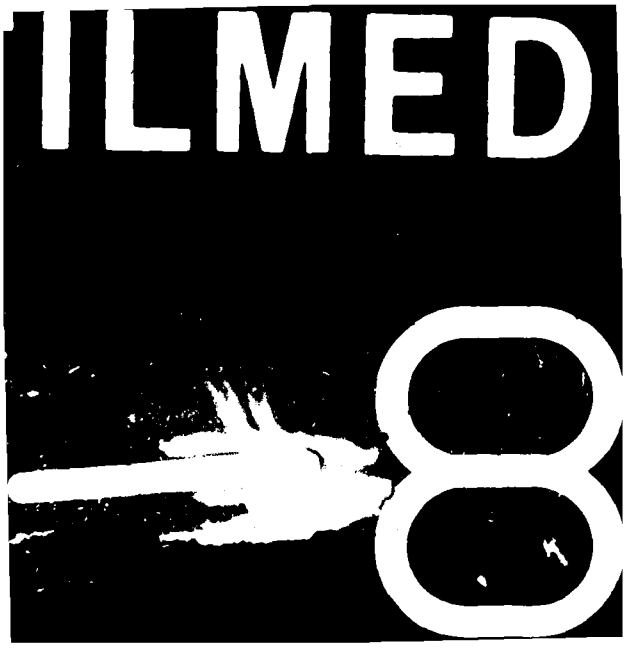
ILMED
8